The Astrophysical Journal, 701:964–973, 2009 August 20 doi:10.1088/0004-637X/701/2/964

THE ACCURACY OF USING THE *ULYSSES* RESULT OF THE SPATIAL INVARIANCE OF THE RADIAL HELIOSPHERIC FIELD TO COMPUTE THE OPEN SOLAR FLUX

M. Lockwood[1,2,4] and M. Owens[3]
[1] Space Science and Technology Department, Rutherford Appleton Laboratory, Chilton, Didcot, Oxfordshire, OX11 0QX, UK; mike.lockwood@stfc.ac.uk
[2] Space Environment Physics, School of Physics and Astronomy, Southampton University, Highfield, Southampton, SO17 1BJ, UK
[3] Blackett Laboratory, Imperial College London, Prince Consort Road, London, SW7 2BZ, UK
Received 2009 April 16; accepted 2009 June 17; published 2009 July 28

ABSTRACT

We survey observations of the radial magnetic field in the heliosphere as a function of position, sunspot number, and sunspot cycle phase. We show that most of the differences between pairs of simultaneous observations, normalized using the square of the heliocentric distance and averaged over solar rotations, are consistent with the kinematic "flux excess" effect whereby the radial component of the frozen-in heliospheric field is increased by longitudinal solar wind speed structure. In particular, the survey shows that, as expected, the flux excess effect at high latitudes is almost completely absent during sunspot minimum but is almost the same as within the streamer belt at sunspot maximum. We study the uncertainty inherent in the use of the *Ulysses* result that the radial field is independent of heliographic latitude in the computation of the total open solar flux: we show that after the kinematic correction for the excess flux effect has been made it causes errors that are smaller than 4.5%, with a most likely value of 2.5%. The importance of this result for understanding temporal evolution of the open solar flux is reviewed.

Key words: interplanetary medium – solar–terrestrial relations – solar wind – Sun: magnetic fields

1. INTRODUCTION

The first survey of the heliosphere outside the ecliptic plane has been carried out by the *Ulysses* spacecraft. In particular, *Ulysses* has observed B_r, the radial component of the magnetic field, as a function of heliocentric distance, r, and heliographic latitude, Λ, and over more than a full solar cycle. It has revealed that the product $|B_r|r^2$ is approximately independent of Λ. This result was first reported in data taken as the spacecraft passed from the ecliptic plane to over the southern solar pole (Smith & Balogh 1995; Balogh et al. 1995). It was then confirmed by the pole-to-pole "fast" latitude scan during the first perihelion pass by the spacecraft (e.g., Lockwood et al. 1999b), the second ascent to the southern polar region (Smith et al. 2001), the second perihelion pass (Smith & Balogh 2003; Smith et al. 2003; Lockwood et al. 2004), and recently the third perihelion pass (Lockwood et al. 2009a). Comparison of the first and second perihelion passes showed that this result held, to a considerable degree of accuracy, under both sunspot minimum and sunspot maximum conditions (Lockwood et al. 2004). Lockwood et al. (2009a) did find a small but consistent difference between the streamer belt and the polar coronal holes during the third perihelion pass, which took place close to sunspot minimum. We investigate this further in the present paper.

This "*Ulysses* result," which is key for understanding the Sun, the heliosphere and its interactions with interstellar space, has been explained in terms of the low plasma beta of the solar wind close to the Sun. This is thought to result in slightly non-radial solar wind flow at low r which acts to equalize tangential pressure and hence the radial magnetic field (Suess & Smith 1996; Suess et al. 1996, 1998). It is an important result because it enables single-point heliospheric observations to be used to quantify the open solar flux leaving the Sun and entering the heliosphere.

Because of this result, the equation for the integrated, signed (of one radial field polarity) heliospheric flux, F_{Sr}, that threads a heliocentric sphere of radius r reduces to

$$F_{Sr} = 2\pi r^2 \langle |B_r|_T \rangle_{CR}. \quad (1)$$

The subscript CR denotes that the averaging is over a full solar (Carrington) Rotation interval, which is required to average out longitudinal structure. T is the timescale on which the B_r data are pre-averaged and then converted into absolute values: T should be chosen so that it is not so large that the opposing field in Toward and Away interplanetary sectors of the field are canceled (which would cause F_S to be underestimated) yet should be large enough to average out small-scale structure in the heliospheric field (which does not reflect structure in the source field and so would cause F_S to be overestimated; Wang & Sheeley 1995; 2002; Lockwood et al. 2006, 2009c). Equation (1) has been used with data taken from near the Earth to study the solar cycle variation of the open solar flux (Wang & Sheeley 1995; Lockwood et al. 1999a, 1999b; Owens et al. 2008a; Lockwood et al. 2009c). In addition, it has been used with historic geomagnetic data to reconstruct the variation of the open solar flux over the past 150 years (Lockwood et al. 1999a; Rouillard et al. 2007; Lockwood et al., 2009c). Lockwood et al. (2004) used data from the first two perihelion passes of *Ulysses*, with simultaneous data from near-Earth spacecraft, to show that the error introduced into F_S estimates from in situ data by the use of Equation (1) was about 5% for averages over a full CR.

Owens et al. (2008a) have recently confirmed the validity of using Equation (1) with data from a single spacecraft by comparing the results from simultaneous observations from widely spaced locations within the heliosphere. This study revealed that neither latitudinal nor longitudinal separations of heliospheric spacecraft ($|\Delta\Lambda|$ and $|\Delta\Phi|$, respectively) introduced significant differences to average estimates of F_S. However, a significant increase in the estimated F_S with heliocentric distance r was found (≈5% per astronomical unit, AU). The "flux excess" ΔF_S is defined as the difference between the signed

[4] Now at Department of Meteorology, University of Reading, Earley Gate, P.O. Box 243, Reading, RG6 6BB, UK.

heliospheric fluxes F_{Sr} and F_{S1} where F_{Sr} is derived (using Equation (1)) from the radial field B_r observed by a spacecraft at general heliospheric coordinates (r, Λ, Φ) and F_{S1} is from the simultaneous radial field B_{r1} derived the same way using observations from near-Earth craft (at $r = r_1 \approx 1$ AU, $\Delta\Lambda \approx 0$, $\Delta\Phi \approx 0$). Using averages over the same solar rotation period, the flux excess is given by

$$\Delta F_S = F_{Sr} - F_{S1} = 2\pi \left\{ r^2 \langle |B_r|_T \rangle_{CR} - r_1^2 \langle |B_{r1}|_T \rangle_{CR} \right\}. \quad (2)$$

The observations of B_r and B_{r1} are here pre-averaged over $T =$ 1 hr intervals before the absolute values are taken to average out small-scale structure in the field. The effect of this averaging timescale, and of sampling effects introduced by solar wind speed variations, has been discussed by Lockwood et al. (2006, 2009a). Lockwood et al. (2009b) used the theory of Burlaga & Barouch (1976) to show that the increase in the flux excess with r found by Owens et al. (2008a) is well explained by the effect of longitudinal structure in the solar wind flow on the frozen-in interplanetary magnetic field.

In the present paper we extend the survey of heliospheric data by Owens et al. (2008a) to investigate the effect of the limited sampling of the heliosphere in space and as a function of the phase of the solar cycle. From this we estimate the error introduced into open flux estimates by using this *Ulysses* result of latitude invariance of the radial field. Before presenting this survey and analysis, in Section 2 we review the applications and implications of the *Ulysses* result.

2. IMPORTANCE OF THE *ULYSSES* RESULT FOR UNDERSTANDING OPEN SOLAR FLUX AND ITS TEMPORAL VARIABILITY

The *Ulysses* result of the latitudinal invariance of the radial component of the heliospheric field is very important because it allows direct quantification of the open solar flux. This has generated a debate (and some unnecessary confusion) about how constant, or otherwise, the open solar flux is on decadal, centennial, and millennial timescales.

A circulation of polar open field lines was proposed by Fisk (1996) as a way of explaining recurrent enhancements of energetic particles seen at high heliographic latitudes but thought to be generated in stream–stream interaction regions at lower latitudes. This circulation generates field lines along which the particles can move to higher latitudes and avoids the need to invoke strong cross-field diffusion. The Fisk circulation allows several phenomena to be explained, at least qualitatively, without the need to invoke any changes in the open flux. However, to suggest that this means that the open flux therefore must be constant is a nonsequitur. A degree of constancy of the open solar flux has been assumed in (as opposed to predicted by) a number of models of the coronal and heliospheric fields solar cycle polarity reversal. Fisk et al. (1999) suggest that continuous or continual reconnection between open and closed flux at coronal hole boundaries allows the polarity reversal to proceed as a rotation of the heliospheric current sheet (HCS), whilst conserving open flux throughout. Fisk & Schwadron (2001) propose that HCS rotation is driven by a diffusive process involving interchange reconnection (which moves the footpoint of an open field line by reconnecting it with a closed field line). Owens et al. (2007) suggest key interchange reconnections occur on the legs of coronal mass ejection (CME) flux tubes, conserving yet transporting open flux in the manner required for the polar coronal hole polarity reversal. These models differ from ideas of variable open flux emergence within active regions, migration to higher latitudes and reconnection with the opposite-polarity open flux of the pre-existing polar coronal hole, remnant from the previous cycle (Schrijver et al. 2002; Wang & Sheeley 2002; Wang et al. 2005; see the review by Lockwood 2004). In this second class of model, the open flux in the heliosphere does not build up continuously (the "flux catastrophe") despite emergence of open flux (in CMEs and other loops) because reconnection between open flux of opposite polarity disconnects flux from the Sun. The differences between these two classes of model have far-reaching implications, well beyond explaining polar coronal hole polarity reversal. Examples of related phenomena include: the origin of the slow solar wind (from the boundaries of coronal holes or from interchange reconnections above the magnetic carpet throughout the streamer belt); the consequent composition of the solar wind; the acceleration of the solar wind (thermal and/or via Alfvén waves and controlled by magnetic flux tube expansion, or the outflow from interchange reconnection sites); and the propagation of cosmic rays through the heliosphere.

If open flux disconnection does occur, and is at a rate that is not matched to its emergence rate (e.g., Owens & Crooker 2007), open flux will not be conserved (Solanki et al. 2000, 2001). Coronal inflows, which may be a signature of disconnection (Wang et al. 1999) exhibit a preference for solar longitudes where the HCS is orientated perpendicular to the solar equator (Sheeley & Wang 2001). Thus the reduction of open flux during recent (particularly the current) solar minima could be the result of the HCS being more warped than in prior cycles, and hence disconnecting a greater amount of open flux. However, note that coronal inflows could also be explained as signatures of interchange reconnection with the loop apex beyond the field of view (e.g., Crooker et al. 2002),

Fisk & Schwadron (2001) justify their assumption of constancy of the open flux on three grounds. Firstly they argue that there is little contact of opposite polarity open flux which would allow open flux to be disconnected. However, footpoint exchange via reconnection with a large emerged loops such as CMEs, or with a series of smaller loops, can readily bring open flux of opposite polarity together (e.g., Lockwood 2004). Secondly, these authors argue that "heat flux dropouts," as could be caused by the loss of streaming electrons from the corona when field lines are disconnected, are rare. Examples of these events are, indeed, hard to find; however, Owens & Crooker (2007) have shown that the sampling of the heliosphere is so sparse that, for the disconnection rates required to explain open flux variations, these events are no rarer than one should expect. Furthermore, scattering of the electrons along long field-aligned path lengths in the heliosphere (and, in particular, at stream–stream interaction regions) means that the electron streams are often absent (in one or both directions) on closed field lines, making identification of disconnection events from these electron dropouts rare (Larson et al. 1997; Fitzenreiter et al. 1998; Owens et al. 2008b). Thirdly, Fisk & Schwadron justify the assumption that the open flux is effectively constant over the solar cycle by noting that the study by Wang et al. (2000), using solar magnetograms and the potential field source surface (PFSS) modeling procedure, shows it to vary by a factor of less than 2 which is considerably smaller than the corresponding variation in the photospheric flux.

Evidence that the open flux does vary, both over the solar cycle and on centennial timescales, has been derived from in situ observations of interplanetary space and from historic geomagnetic data by Lockwood et al. (1999a, 1999b, 2009c), Lockwood (2001, 2003), and Rouillard et al. (2007). All these estimates use the *Ulysses* result, the accuracy of which is evaluated in the present paper. The recent paper by Lockwood et al. (2009c) shows that solar cycle variations in open flux are indeed typically by a factor 2 (as noted from PFSS data by Wang et al., 2000) and that since 1905 the lowest annual mean open flux derived (in 1913) was 1.22×10^{14} Wb and the largest (in 1991) was 5.65×10^{14} Wb (and values exceeding 5.55×10^{14} Wb were seen in 1957 and 1982 as well as 1991). Thus the recent centennial and solar cycle variations combine to give a variation in open flux by a factor of about 4.5. Studies using cosmogenic isotopes show that on millennial scales even larger amplitude variations in open solar flux are expected (McCracken, 2007).

It has been claimed that the deduced rise in open flux over the past century is an artifact caused by errors in the aa geomagnetic index (Svalgaard et al. 2003, 2004) or was present but with only a small magnitude (Svalgaard & Cliver 2005). However, Rouillard et al. (2007) and Lockwood et al. (2009c) use an aa index that has been corrected using other range geomagnetic indices (and not using hourly mean data which often display a different dependence on interplanetary parameters) and find a doubling of the mean open flux on centennial timescales. Nevertheless, Svalgaard & Cliver (2007) even argue that the solar minimum open flux has for recent cycles been at a minimum "floor" value of 4×10^{14} Wb (in annual means), in other words that there is no centennial variation in open flux at all. This idea is in direct contradiction with the decline in open flux seen over the last two solar cycles in interplanetary data: Lockwood et al. (2009a, 2009c) used the *Ulysses* result to show that for the sunspot minimum years of 1985, 1997, and 2008, the annual mean open solar flux was 3.57×10^{14} Wb, 2.51×10^{14} Wb, and 1.80×10^{14}, respectively (the last two well below Svalgaard & Cliver's "floor" value of 4×10^{14} Wb). Thus the open flux at sunspot minimum was twice as large just two solar cycles ago than during the recent minimum. The reasons for the radically different conclusions about open flux variability of Svalgaard & Cliver and of Lockwood et al. are discussed in Lockwood et al. (2006), Rouillard et al. (2007), and Lockwood et al. (2009c).

The long-term changes in the open flux deduced from geomagnetic activity by Lockwood et al. (1999a, 1999b, 2009c), Lockwood (2001, 2003), and Rouillard et al. (2007) have been reproduced by a number of analytic or numerical models of flux continuity and transport during the solar magnetic cycle, given the variation in photospheric emergence rate indicated by sunspot numbers (Solanki et al. 2000, 2001; Schrijver et al. 2002; Lean et al. 2002; Wang & Sheeley 2002; Wang et al. 2005). The principle established by Solanki et al. is that total open flux F_S obeys a continuity equation, with the rate of change being the difference between the source terms (the total rate that coronal field loops emerge through the coronal source surface—including CMEs) and loss terms due to field reconfiguration and disconnection by magnetic reconnection. In the absence of known mechanisms that could make the total loss (from the variety of mechanisms) exactly equal to the simultaneous production rate, we must expect the total open flux to vary on a variety of timescales.

Fisk & Schwadron (2001) do note that their theory does not require the open flux to be rigorously constant and that there is undoubtedly new flux emergence in CMEs and disconnection by reconnection between opposite polarity open flux: what they do assume is that these effects give variations on timescales greater than the characteristic timescales of the proposed open flux transport mechanisms. There is no obvious reason to think this is not a valid assumption for the purposes of their theory but adopting it does not imply that the open solar flux does not vary on timescales of several solar rotations up to millennia.

Lastly, we note that the current low solar minimum is part of a trend that was noted by Lockwood (2001, 2003) in declining open solar flux since 1986. Lockwood & Fröhlich (2007) analyzed this trend using running solar cycle averages and compared it to matching trends in other solar activity indicators such as sunspot number, cosmic ray fluxes, and total solar irradiance. They also discussed the implications of these trends for our understanding of solar variability contributions to recent global climate change.

3. OBSERVATIONS

For the data considered here to be away from the Earth, i.e., observations at general (r, Λ, Φ) coordinates, we employ all of the data set described by Owens et al. (2008a), with data from the magnetometers on board the following satellites: *Pioneer 6* (Ness et al. 1966); *Pioneer 7* (Ness et al. 1966); *Pioneer 10* (Smith et al. 1975); *Pioneer 11* (Smith et al. 1975); *Helios 1* (Scearce et al. 1975); *Helios 2* (Scearce et al. 1975); *Voyager 1* (Behannon et al. 1977); *Voyager 2* (Behannon et al. 1977); *Pioneer Venus Orbiter* (Russell et al. 1980); *ICE* (*ISEE 3* after it was moved from orbit around the L1 Lagrange point) (Frandsen et al. 1978); *Ulysses* (Balogh et al. 1992); *NEAR* (Acuña et al. 1997); *STEREO A* (Acuña et al. 2007) and *STEREO B* (Acuña et al. 2007). These spacecraft contribute heliospheric flux values that we call F_{Sr}. The simultaneous data from near-Earth craft (at $r = r_1 \approx 1$ AU, $\Delta\Lambda \approx 0$, $\Delta\Phi \approx 0$), are all taken from the OMNI data set maintained by the Space Physics Data Facility at Goddard Space Flight Center. These data originate from craft within interplanetary space, either in Earth orbit or in a halo orbit around the L1 Lagrange point. The data have been lagged to the nose of Earth's magnetosphere using the observed solar wind speed and inferred orientation of interplanetary structures. In recent years, the data are exclusively from the magnetometers on board the *IMP 8* (Mish et al. 1964), *Wind* (Lepping et al. 1995), and *ACE* (Smith et al., 1998) spacecraft. Earlier OMNI magnetic field data come from *IMP 1* (Ness et al. 1964); *IMP 3* (Ness et al. 1964); *AIMP 1* (Behannon 1968); *IMP 4* (Fairfield 1969); *AIMP 2* (Ness et al. 1967); *HEOS 1* (Hedgecock 1975); *IMP 5* (Fairfield & Ness 1972); *IMP 6* (Fairfield 1974); *IMP 7* (Mish & Lepping 1976); *Prognoz 10* (Stayzhkin et al. 1985); *ISEE 3* (*ICE* before it was moved from L1) (Frandsen et al. 1978); and *Geotail* (Kokubun et al. 1994). The OMNI data set contributes heliospheric flux values (using Equation (1)) that we term F_{S1}.

The different orbits of the various spacecraft employed here mean that the solar rotation periods in their rest frames differ slightly. For example, it is 27.275 days as seen from Earth and the L1 Lagrange point, but for *Ulysses* it is near 26 days. We employ averages over common 27 day (Bartels) rotation intervals for all craft. Hence we do not attempt to make allowance for the slightly different solar rotation periods, as seen in their various frames of reference, nor do we include any solar wind propagation delays between r_1 and r. The full data set used here extends out to r of 20 AU.

Figure 1 shows a scatter plot of Bartels rotation (27 day) means of F_{Sr} as a function of those of F_{S1} for the whole data

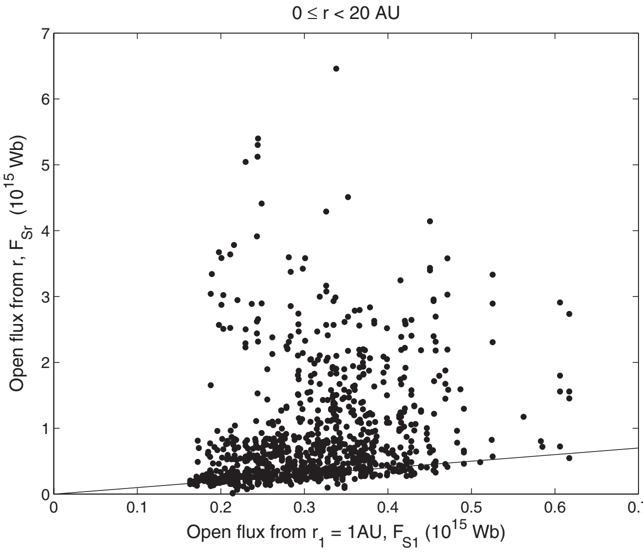

Figure 1. Scatter plot of averages over Bartels Rotations of the heliospheric flux derived from near Earth observations (at $r = r_1 = 1$ AU) from the OMNI data set, $F_{S1} = 2\pi r_1{}^2 <|B_{r1}|_T>$, compared with simultaneous observations made elsewhere in the heliosphere (at different heliocentric distance r, and/or heliographic longitude, Φ, and/or and heliographic latitude, Λ), $F_{Sr} = 2\pi r^2 <|B_r|_T>$. This plot is for all data at $r \leqslant 20$ AU. The absolute values are taken on a timescale T of 1 hr throughout this paper. The solid line is $F_{S1} = F_{Sr}$.

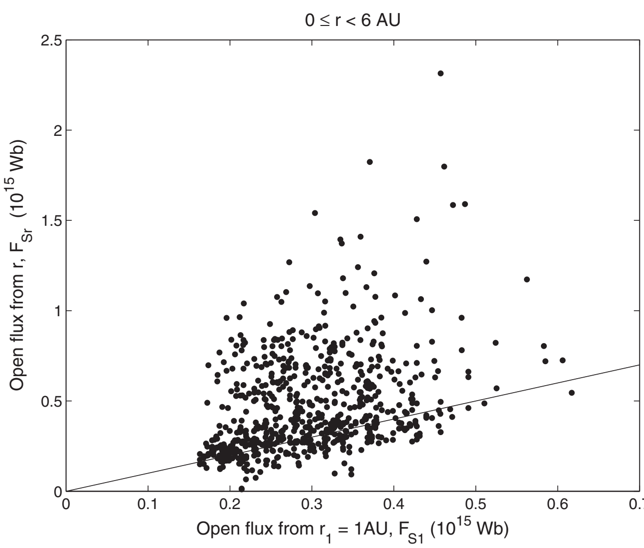

Figure 2. Same as Figure 1 for $r \leqslant 6$ AU.

set, irrespective of the spacecraft separations in r, Λ, or Φ. The solid line is $F_{Sr} = F_{S1}$. It can be seen that there is considerable scatter, with many points giving $F_{Sr} \gg F_{S1}$. Owens et al. (2008a) showed that the excess flux $\Delta F_S = F_{Sr} - F_{S1}$ increases with increasing r and this is confirmed in Figures 2 and 3 of the present paper. Figure 2 is the same as Figure 1 but for data at $r < 6$ AU. The largest outliers are removed; however, the scatter is still great.

The variation of the flux excess ΔF_S with r is shown in Figure 3. This plot shows that the rise in ΔF_S with r appears to be nonlinear and the scatter also increases greatly with r. As pointed out by Owens et al. (2008a), this is the dominant variation found in the data and care must be taken to ensure aliasing of this variation, caused by limited sampling, does not give apparent variations with other parameters. The solid line in

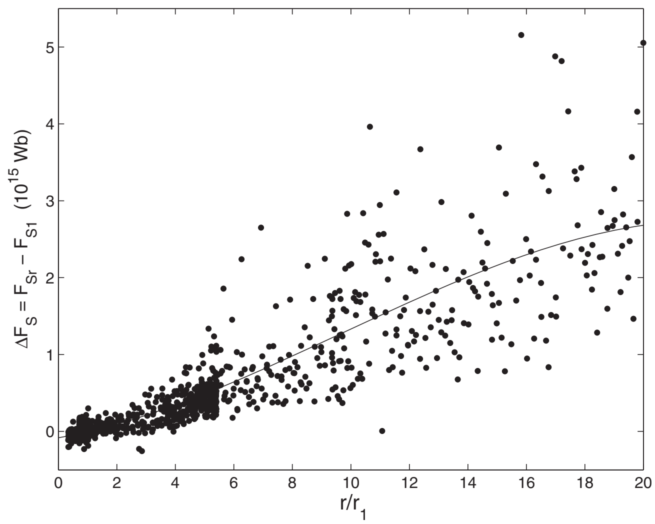

Figure 3. Bartels rotation averages of the flux excess $\Delta F_S = F_{Sr} - F_{S1} = 2\pi(r^2|B_r| - r_1{}^2|B_{r1}|)$, as a function of r (in AU) for data at all heliographic latitudes Λ and longitudes Φ. The solid line is a third-order polynomial fit, $1/C(r)$.

Figure 3 is a third-order polynomial fit to the data points, which we call $1/C(r)$. (The best fit polynomial is $C^{-1}(r) = -0.0832 + 0.0675r + 0.0113r^2 - 0.0004r^3$, where r is in AU).

Figure 4(a) shows the scatter plot of the flux excess ΔF_S against the absolute value of the difference in heliographic latitudes between the two measurements, $|\Delta\Lambda|$. Figure 4(b) investigates the interdependence of the sampling of $|\Delta\Lambda|$ and r. The high-latitude *Ulysses* data are readily identifiable in these plots as they are the only data to extend above $|\Delta\Lambda| = 30°$. Figure 4(b) also shows that these *Ulysses* data points come from a range of r and the perihelion pass data can be distinguished from data from the remainder of the orbit. Figure 4(a) shows that *Ulysses* ΔF_S data are very similar across the full range of $|\Delta\Lambda|$, although careful inspection does reveal the effect of r with the spread ΔF_S being higher at $|\Delta\Lambda| = 30°$ (for which the range of r is greater) than for the largest $|\Delta\Lambda|$ (85°, where all samples come from r close to 2 AU). The data in Figure 4 from the highest r come for the two *Voyager* crafts and *Pioneer 11* and it can be seen in Figure 4(b) that as their r increased, their excursions to higher $|\Delta\Lambda|$ have become larger. Note that a threshold for higher latitude observations of $|\Delta\Lambda| = 30°$ excludes these large-r data points.

Figure 5 shows the corresponding plot for the heliographic longitude difference $|\Delta\Phi|$. No dependence of ΔF_S on $|\Delta\Phi|$ can be seen, which shows that averaging over 27 day solar rotation periods has been effective in removing longitudinal structure, at least on average. The sampling in (r, $|\Delta\Phi|$) space shown in Figure 5(b) is very uniform, the only structure being a very slight concentration of data points from near Earth ($r \approx r_1$ and $|\Delta\Phi| \approx 0$)

4. VARIATIONS OVER THE SUNSPOT CYCLE

Figure 6 is the same format as Figures 4 and 5 for the mean sunspot number R over the 27 day intervals. On first inspection of Figure 6(a), it appears that the largest excess flux values do not occur at the largest sunspot numbers. However, inspection of Figure 7(b) shows this is likely to be an artifact of the variation with r, as the data from the greatest r come from lower sunspot numbers (i.e., the craft were at $10 < r < 20$ AU during relatively low sunspot activity periods: in fact the progress of the declining

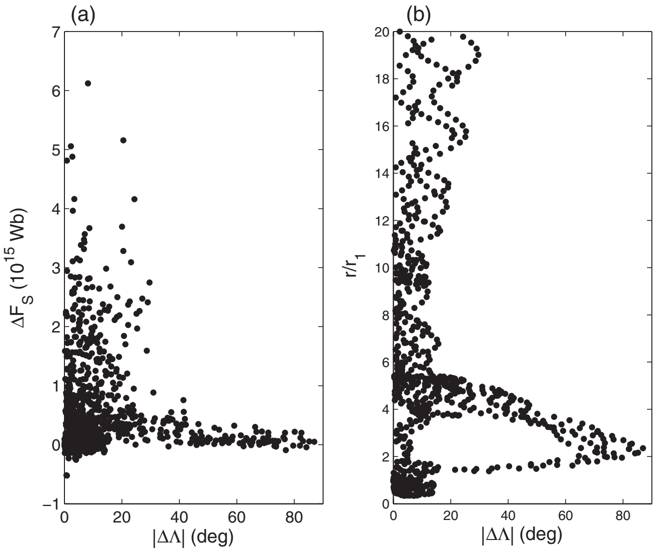

Figure 4. (a) Bartels rotation averages of the flux excess $\Delta F_S = F_{Sr} - F_{S1} = 2\pi(r^2|B_r| - r_1{}^2|B_{r1}|)$, as a function of the absolute value of the difference in heliographic latitude with respect to Earth, $|\Delta\Lambda|$, for data at all heliographic longitudes Φ and at $r \leqslant 20$ AU. In (b) r/r_1 is plotted as a function of $|\Delta\Lambda|$ for these observations. ($r_1 = 1$ AU).

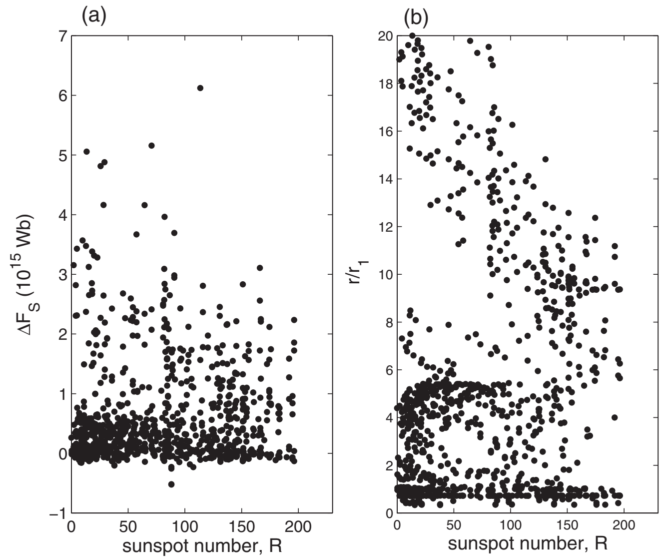

Figure 6. Same as Figure 4 but for the sunspot number, R. (a) ΔF_S as a function of R for data at all heliographic latitudes Λ and longitudes Φ and at $r \leqslant 20$ AU. (b) r/r_1 as a function of R.

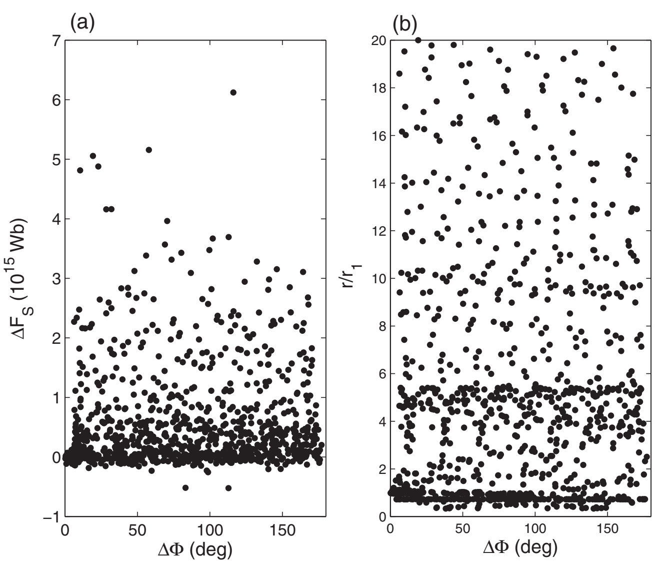

Figure 5. Same as Figure 4 but for the heliographic longitude, relative to the Earth, $|\Delta\Phi|$. (a) ΔF_S as a function of $|\Delta\Phi|$ for data at all heliographic latitudes Λ and at $r \leqslant 20$ AU. (b) r/r_1 as a function of $|\Delta\Phi|$.

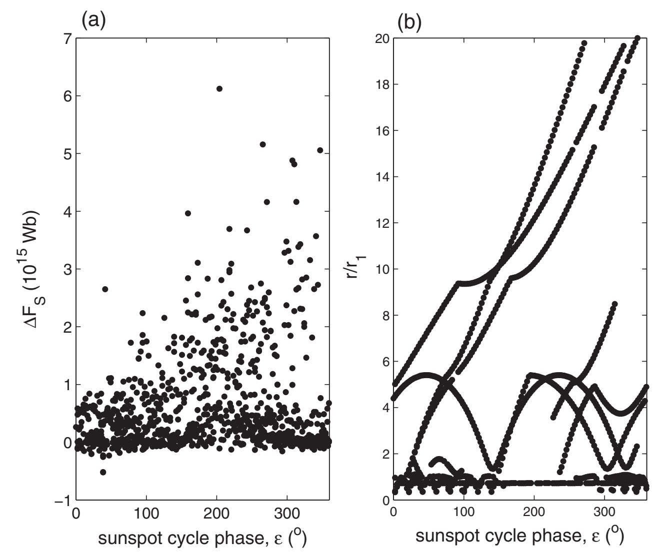

Figure 7. Same as Figure 4 but for the sunspot cycle phase, ε. (a) ΔF_S as a function of ε for data at all heliographic longitudes Φ, heliographic latitudes $\Lambda \leqslant 30°$ and $r \leqslant 20$ AU. (b) r/r_1 as a function of ε for the same data subset.

phase can clearly be detected in Figure 6(b) as the *Voyager* and *Pioneer 11* spacecrafts moved to greater r). The data from $r \leqslant 2$ AU are somewhat biased to low solar activity intervals but the full range of R is covered. The data from 4 AU $< r \leqslant 6$ AU are quite strongly biased to lower R.

Although R can discriminate between solar minimum and solar maximum, it cannot differentiate between the rising and falling phases of the solar cycle. To achieve this, we define the start of each sunspot cycle, following each minimum, by the onset of the first consistent rise of R above a threshold of 20 in 27 day means and define this time t_o to be zero solar cycle phase (ε). The length L of each cycle is then determined from the interval between successive $\varepsilon = 0$ points and the phase at a time t within that cycle obtained from the simple linear relation $\varepsilon = 2\pi(t - t_o)/L$. Figure 11(d) shows the variation with ε of the average sunspot number. This sunspot cycle variation is typical of individual cycles in that the maximum in these means of R is near $\varepsilon = 100°$, after which there is a declining phase which lasts considerably longer than the rising phase. There is a secondary peak in the mean R values (the interval between it and the main peak often being called the Gnevyshev Gap).

Figures 7 and 8 are in the same format as Figures 3–6, but for the solar cycle phase, ε. Figure 7 is for all the data at $\Lambda \leqslant 30°$ (dominated by data within the streamer belt), Figure 8 is for $\Lambda > 30°$, these higher latitude data coming entirely from *Ulysses*. Again, initial inspection of Figure 7(a) implies that the occurrence of the larger ΔF_S values increases with sunspot cycle phase right the way up to the start of the new cycle ($\varepsilon = 2\pi$); however, Figure 9(b) shows that this is again dominated by the large r data from *Voyager* and *Pioneer 11* which are all from the declining phase: for these observations, ε increases as r increases. A lack of samples for $r \leqslant 2$ AU in the early declining phase (ε between about 150° and 250°) can be seen.

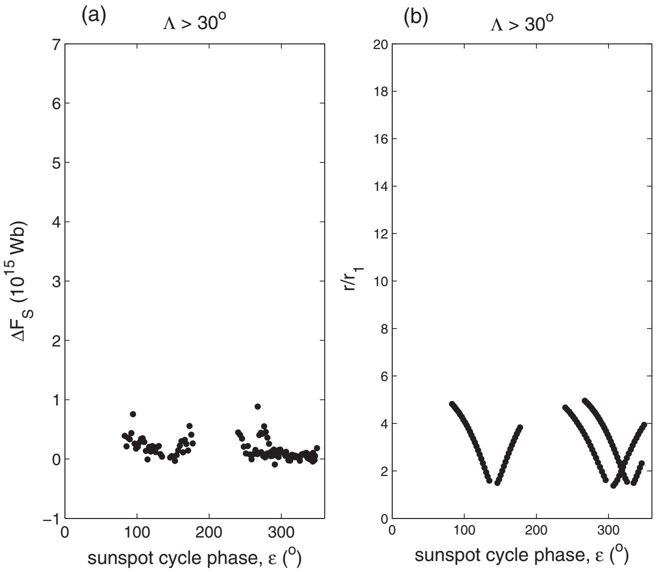

Figure 8. Same as Figure 7 for heliographic latitudes $\Lambda > 30°$. Note that these data are all provided by the *Ulysses* spacecraft.

Figure 8 is the same as Figure 7, but for $\Lambda > 30°$, data for which come entirely from *Ulysses*. The variability in the flux excess can be seen to be controlled by r because the patterns in the r–ε plot (Figure 8(b)) are somewhat mirrored in the ΔF_S-ε plot (Figure 8(a)). However, this is not completely true and close inspection shows that rises in r have more effect on ΔF_S at ε of about 150°–300° (declining phase) than they do at both lower and higher ε.

5. DISCUSSION

In this section, we use the fitted polynomial $C^{-1}(r)$ in Figure 3 to remove the average variation with r. We need to do this in order to obtain sufficient samples to survey the variations of excess flux with other parameters such as $|\Delta\Lambda|$, $|\Delta\Phi|$, R and ε. We here make use the r-corrected open flux ratio:

$$\eta = C(r) \cdot F_{Sr}/F_{s1} \tag{3}$$

where $C^{-1}(r)$ is the fitted polynomial in Figure 3. Figure 9 plots η for samples taken at $r \leqslant 6$ AU as a function of (a) latitude difference $|\Delta\Lambda|$, (b) longitude difference $|\Delta\Phi|$, and (c) heliocentric distance r. The gray dots are the individual 27 day samples and the black histogram line shows means in equal width bins of $|\Delta\Lambda|$, $|\Delta\Phi|$, and r (for 9(a), (b), and (c), respectively). Figure 9(c) shows the normalization using $C(r)$ has been effective in completely removing the r dependence in the means because mean η is unity at all r. Although the variability in mean η rises with increasing longitudinal separation $|\Delta\Phi|$ there is no coherent change from unity. On the other hand, there is a marked and coherent drop in the variation of the mean η with latitudinal separation at about $|\Delta\Lambda| = 40°$, showing that the high-latitude data give η consistently below unity.

Figure 10 shows the distributions of the Bartels rotation means of η for F_{Sr} values measured at $r < 6$ AU and: (a) all latitudes, (b) $|\Delta\Lambda| \leqslant 2°$ and (c) $|\Delta\Lambda| > 40°$. Ideally, η would be unity at all locations, from the point of view of applying Equation (1). Although this is true for the mean of the whole data set (Figure 10(a)), Figure 10 shows that there are some large deviations from unity. It is thus worth considering the potential sources of this:

1. Inaccurate intercalibration of the pairs of magnetometers employed would lead to differences between and B_r and B_{r1} (and hence F_{Sr} and F_{S1}) (Petrinic & Russell. 1993).
2. The use of fixed 27 day averaging intervals means that different craft are not studying precisely the same range of Carrington longitudes. To achieve this, the start times of the intervals used would need to be varied to account for the longitude difference $|\Delta\Phi|$ and differences in the propagation delay from 1 AU to r (which depend on r and the solar wind speed). In addition, the length of the interval needed

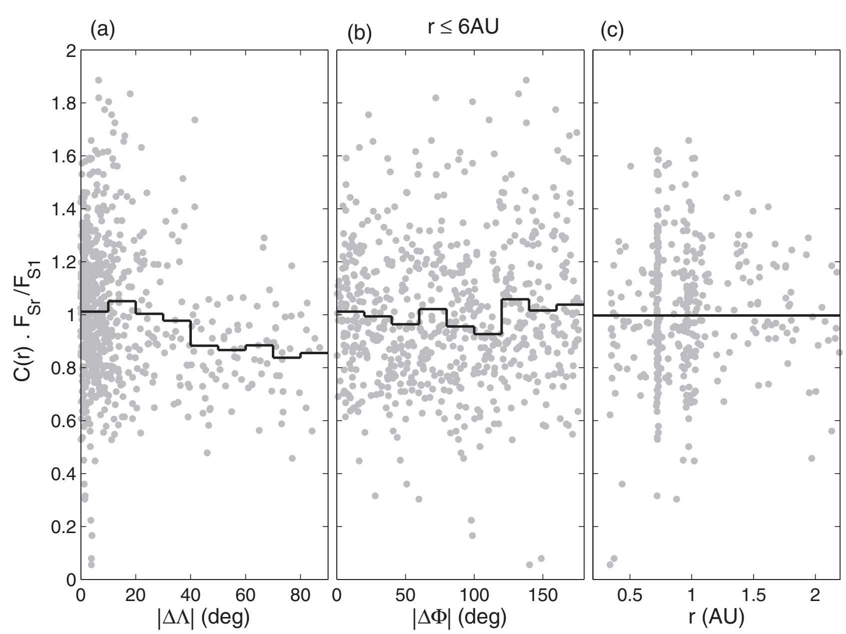

Figure 9. Scatter plots of the r-corrected ratio $\eta = C(r)F_{Sr}/F_{S1}$ at $r \leqslant 6$ AU as a function of (a) heliographic latitude difference $|\Delta\Lambda|$; (b) heliographic longitude difference $|\Delta\Phi|$ and (c) heliocentric distance r. Gray dots are individual 27 day data points and the histograms are means in nine equal-sized bins that cover the full range in each case.

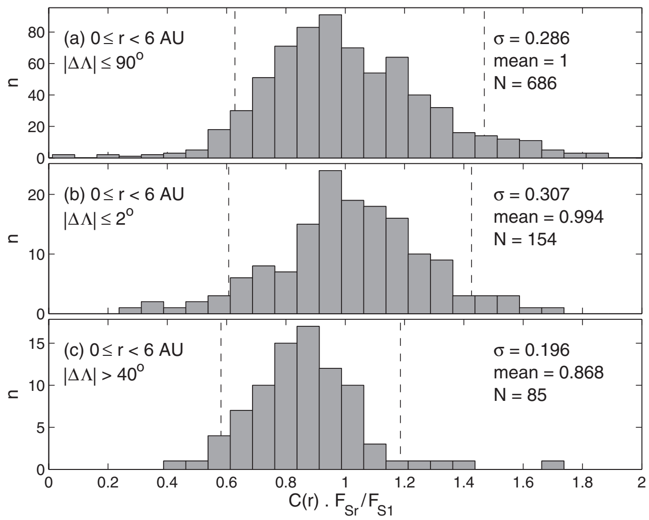

Figure 10. Distributions of $\eta = C(r) \cdot F_{\mathrm{Sr}}/F_{\mathrm{S1}}$ at $r \leqslant 6$ AU: n is the number of samples in equal width bins. The observed flux ratios at r have been corrected to $r = r_1$ by the factor using $C(r)$ from the polynomial fit shown in Figure 3. (a) for all samples, $|\Delta\Lambda| \leqslant 90°$; (b) for samples close to the latitude of Earth, $|\Delta\Lambda| \leqslant 2°$; (c) for high latitude samples, $|\Delta\Lambda| > 40°$. In each panel, the standard deviation, σ, the total number of samples, N, and the mean of the distribution are given. Vertical dashed lines are the 2σ points for each distribution.

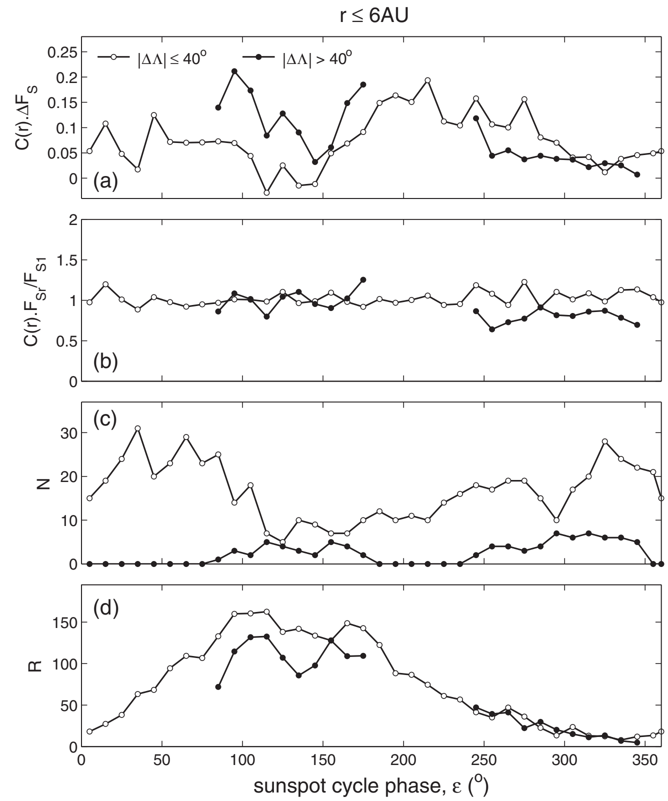

Figure 11. Variations with sunspot cycle phase, ε. (a). The r-corrected flux excess $C(\mathrm{r}).\Delta F_{\mathrm{S,}}$ averaged over 10° bins of sunspot cycle phase, ε, as a function of ε for all data at $r \leqslant 6$ AU. The line connecting open points is for $|\Delta\Lambda| \leqslant 40°$, the line connecting filled points are for $|\Delta\Lambda| > 40°$ (where sufficient data exist). (b) mean values of the corrected ratio $\eta = C(r) \cdot F_{\mathrm{Sr}}/F_{\mathrm{S1}}$ in the same bins; (c) the number of samples, N, contributing to the means. (d) The mean sunspot numbers, R, in the same bins.

to cover a 360° range of Carrington longitudes depends on the longitudinal motion of the craft in question.

3. Temporal variations in the heliospheric field and/or the longitudinal solar wind velocity structure (the latter via the kinematic effect which introduces the flux excess) would lead to differences seen by craft at different solar longitudes. This temporal effect means that any modifications to fixed 27 day intervals suggested by (2) above have little effect in reducing the spread of η values.
4. There is an uncertainty introduced by the use of $C(r)$ to make a correction for r. This could be avoided only if we had sufficient samples to use averaging bins with a small width in r.
5. Any limitations to the *Ulysses* result on the latitude invariance of the radial field would also cause and $\eta = C(r) \cdot F_{\mathrm{Sr}}/\mathrm{Fs}_1$ to vary from unity for the data from larger $|\Delta\Lambda|$.

To investigate the role of (5), relative to other effects, Figure 10(b) looks at the distribution of the derived η for craft near the Earth's latitude ($|\Delta\Lambda| \leqslant 2°$ and all $|\Delta\Phi|$, for which there are $N = 154$ samples for $r < 6$ AU). The mean of the distribution is very close to unity, but the spread is large (standard deviation $\sigma = 0.31$ and the error at the 2σ level is 0.41). This spread is very close to that seen in the overall data set (Figure 10(a)) but cannot be caused by latitudinal variation (effect 5) as $|\Delta\Lambda| \leqslant 2°$. Thus the spread in the overall data set must be mainly due to effects 1–4 and not to effect 5. Figure 10(c) is, on the other hand, subject to the error 5 because it is for $|\Delta\Lambda| > 40°$. The spread for these 85 samples is considerably smaller (standard deviation $\sigma = 0.15$ and error at the 2σ level of 0.30). Thus any additional random error due to effect 5 incurred by moving to higher latitudes is considerably smaller than a net reduction in the other random errors (effects 1–4). We note that there is a systematic shift outside the streamer belt (the mean of the η distribution in Figure 10(c) is 0.87 rather than unity, which is also seen in Figure 9(a)).

This systematic effect (lower mean value of η for the $|\Delta\Lambda| > 40°$ data subset) is expected for the kinematic excess flux effect discussed by Lockwood et al. (2009b) because for $|\Delta\Lambda| < 40°$, F_{Sr} values, like the F_{S1} ones, are taken within the streamer belt (where the mixture of fast and slow solar wind makes the kinematic flux excess effect large—especially during the declining phase of the solar cycle when polar coronal hole extensions reach down to low Λ). On the other hand, the F_{Sr} values for the $|\Delta\Lambda| > 40°$ data are largely from within the polar coronal holes where stream–stream interactions are generally less important: the exception to this is at sunspot maximum when fast and slow solar wind are seen at all latitudes (McComas et al. 2003).

From the above, it becomes important to look at the distribution of available samples in both latitude ranges with sunspot cycle phase. This is presented in Figure 11. From top to bottom, the panels show, as a function of ε: (a) the means of r-corrected flux excess $C(r)\ \Delta F_{\mathrm{Sr;}}$ (b) the means of r-corrected flux ratio, $\eta = C(r) \cdot F_{\mathrm{Sr}}/F_{\mathrm{S1}}$; (c) the number of samples in each mean, *N;* and (d) the mean sunspot number, R. In each case we employ 10°-wide bins in solar cycle phase ε. The data for $|\Delta\Lambda| > 40°$ are shown by filled circles those for $|\Delta\Lambda| \leqslant 40°$ by open circles.

Considering first the low-latitude data, the open circles in Figure 11(c) show that although we have observations at all ε, the sampling is not uniform, with relatively few samples at sunspot maximum and during the declining phase. Figure 11(a) shows that the flux excess effect is actually a minimum at sunspot maximum, presumably because the many stream–stream interactions at these times cause the fast solar wind to be slowed and the slow solar wind to be speeded up and so the differences are reduced (McComas et al. 2003). The mean flux excess is greatest for these streamer belt data during the declining phase when fast flow in low-latitude coronal hole extensions reaches down into the streamer belt most frequently. Figure 11(b) shows that this solar cycle variation in the flux excess has no effect on the mean values of $\eta = C(r) \cdot F_{Sr}/F_{S1}$ because both spacecraft are in the streamer belt and F_{Sr} and F_{S1} are proportionally affected by the kinematic flux excess effect.

For the high-latitude data (solid circle data points), the situation is different in many respects. Firstly, Figure 11(c) shows that the sampling is restricted to near sunspot maximum and minimum. This is because these latitudes have only been addressed by *Ulysses* at these times (in fact, twice near sunspot minimum, once near sunspot maximum and Figure 11(d) shows that the maximum was a relatively weak one compared to those for other cycles in the survey). The absolute flux excess in Figure 11(a) again appears to show a minimum at sunspot maximum, but the values are greater than seen at lower latitudes. On the other hand, in the late declining phase in Figure 11(a), the absolute flux excess is lower at than at low latitudes. These differences cause the difference in the behavior of η shown in Figure 11(b). At sunspot maximum the effect on F_{Sr} and F_{S1} is the same, as it is at all times at low latitudes. This is expected because the mix of fast and slow solar wind at this time does not depend on latitude (McComas et al. 2003). However, at sunspot minimum, the lower values of $\eta = C(r) \cdot F_{Sr}/F_{S1}$ are to be expected at higher latitudes because F_{Sr} is recorded within the large polar coronal hole, where flows are uniformly fast (and so there is little enhancement by the kinematic flux excess effect); on the other hand, F_{S1} is measured within the streamer belt and continues to be enhanced by this effect. Hence η falls for the large $|\Delta\Lambda|$ data at sunspot minimum. Because there are more samples around sunspot minimum than sunspot maximum in our survey, we see a fall in the overall mean values of η at $|\Delta\Lambda| > 40°$ in Figures 9 and 10. The mean value of η at $|\Delta\Lambda| > 40°$ and $\varepsilon > 200°$ is 0.796. For the times when the sunspot minimum data studied here were recorded by *Ulysses*, the flux excess for near-Earth measurements, as computed by Lockwood et al. (2009b), gave a mean value $<(F_{S1} - \Delta F_{S1})/F_{S1}> = 0.750$. Thus the survey presented here is consistent with the flux excess effect being almost completely absent at high latitudes during sunspot minimum but being the same as within the streamer belt at sunspot maximum.

This conclusion is strongly supported by the distributions of $\eta = \mathrm{C}(r) \cdot F_{Sr}/F_{S1}$ shown in Figure 12. These are shown in the same format as in Figure 10 but are for different subsets of the data. Figure 12(a) is for all samples at $0.8 < r \leqslant 1.2$ AU and $|\Delta\Lambda| \leqslant 40°$ (i.e., at r close to 1 AU and at low latitudes, within in the streamer belt), whereas (b) is for samples at $r \leqslant 6$ AU, $|\Delta\Lambda| > 40°$ and $70 \leqslant \varepsilon < 190°$ (i.e., the high-latitude set at sunspot maximum) and (c) is for samples at $r \leqslant 6$ AU, $|\Delta\Lambda| > 40°$ and $240 \leqslant \varepsilon < 360°$ (i.e., the high-latitude set at sunspot minimum). The distribution in Figure 12(a) has a mean of 1.02, a standard deviation σ of 0.25, and a spread at the 2σ level of 0.38. That in Figure 12(b) has a mean of 0.99, σ of 0.22, and a spread at the 2σ level of 0.35. The distribution in (b) is therefore very similar to that in (a), the main difference being that it contains just $N = 31$ samples compared to the $N = 132$ contributing to (a). Thus there is no evidence here for a significant difference between the low latitude case and higher latitudes at sunspot maximum. The distribution in (c) is, however, significantly different: it has a mean of 0.80, σ of 0.14, and a spread at the 2σ level of 0.23 (it is made up from more samples than (b) with $N = 54$). In addition

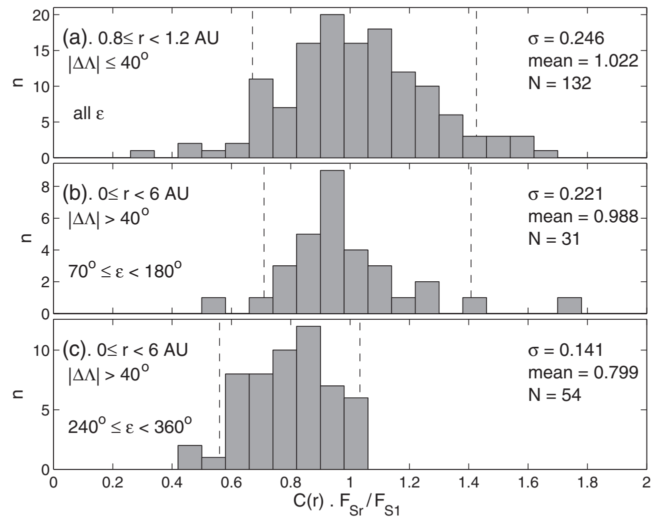

Figure 12. Distributions of the ratio $\eta = C(r) \cdot F_{Sr}/F_{S1}$, as in Figure 10, for: (a) for all samples at $0.8 < r \leqslant 1.2$ AU and $|\Delta\Lambda| \leqslant 40°$; (b) $r \leqslant 6$ AU and $|\Delta\Lambda| > 40°$ at sunspot maximum (all samples come from the range of sunspot phases $70 \leqslant \varepsilon < 190°$); (c) $r \leqslant 6$ AU and $|\Delta\Lambda| > 40°$ at sunspot minimum (all samples come from the range $240 \leqslant \varepsilon < 360°$).

to the lower mean found in Figure 11, Figure 12(c) shows the spread about the mean is halved at sunspot maximum when the away-from-1 AU craft is within a large polar coronal hole.

6. CONCLUSIONS

Our results show that the accuracy of the *Ulysses* result of the latitudinal invariance of the radial field is much greater than might appear from the comparison of results from pairs of spacecraft. The "flux excess" effect means that the $r^2|B_r|$ increases with heliocentric distance and this has been explained by Lockwood et al. (2009a, 2009b) in terms of the kinematic effect on the frozen-in magnetic field of longitudinal structure in the solar wind flow. Making allowance for the average increase with r, we here find the that scatter in the comparison between two spacecraft is halved when one of the pair is at high latitudes within a large sunspot-minimum polar coronal hole (where the flow is spatially uniform and the kinematic effect is found to be small). Thus the scatter in the comparison between two craft appears to be dominated by the variability of the flux excess effect. We can find no evidence for latitudinal variability in the source radial field (before it is enhanced by the kinematic effect). Hence adoption of Equation (1) introduces errors that must be at least an order of magnitude smaller than those caused by the flux excess effect. As the latter are typically 38% at the 2σ level (as, e.g., in Figure 12(a)), we infer the error introduced by any variability in the latitudinal profile of radial field must be something less than the 5% which Lockwood et al. (2004) derived for 27 day means during the first two perihelion passes of *Ulysses*.

We can quantify this error more precisely using Figure 12. The flux excess effect means that the observed radial fields at the two craft are $B_r = B_{ro} + \Delta B_r$ and $B_{r1} = B_{ro1} + \Delta B_{r1}$, where the true source fields are B_{ro} and B_{ro1} and the kinematic correction terms are ΔB_r and ΔB_{r1}. If we call the ratio of the true radial source fields $f(\Lambda) = B_{ro}/B_{ro1}$, we can express the observed r-corrected ratio (Equation (3)) as

$$\begin{aligned}\eta &= CF_S/F_{S1} = CB_r/B_{r1} \\ &= C\gamma(B_{ro} + \Delta B_r)/(B_{ro1} + \Delta B_{r1}) = C\gamma f A A_1 \end{aligned} \quad (4)$$

where $A = (1 + \Delta B_r/B_{ro})$ and $A_1 = (1 + \Delta B_{r1}/B_{ro1})$ and γ allows for any calibration difference between the magnetometers on the two craft (Petrinic & Russell 1993). We can use (4) to compute the uncertainty in η:

$$(\sigma_\eta/\eta)^2 = (\sigma_f/f)^2 + (\sigma_C/C)^2 + (\sigma_\gamma/\gamma)^2 + (\sigma_A/A)^2 + (\sigma_{A1}/A_1)^2. \tag{5}$$

For random, but no systematic, errors due to instrument intercalibration and the *Ulysses* result, γ and f are unity but σ_f and σ_γ are nonzero. Consider the distribution in Figure 12(a), for which $\sigma_\eta = 0.246$ and $\langle\eta\rangle = 1.022$. Because these data are taken from the same latitude (to within $|\Delta\Lambda|$ of $2°$), $\sigma_f = 0$ in this case. Also because the two measurements are essentially at the same latitude and r, $\sigma_C = 0$ ($C = 1$) and $(\sigma_A/A)^2 = (\sigma_{A1}/A_1)^2$, hence (5) becomes for this case

$$(0.246/1.022)^2 = (\sigma_\gamma/\gamma)^2 + 2(\sigma_{A1}/A_1)^2. \tag{6}$$

On the other hand, for the distribution in Figure 12(c), $\sigma_\eta = 0.141$ and $\langle\eta\rangle = 0.799$. In this case, we can consider σ_A to be zero because the satellite is in the sunspot minimum polar coronal hole where the flow is uniform and in the previous section we inferred the flux excess was very close to zero. Hence Equation (5) applied to this case yields

$$(0.141/0.799)^2 = (\sigma_f/f)^2 + (\sigma_C/C)^2 + (\sigma_\gamma/\gamma)^2 + (\sigma_{A1}/A_1)^2. \tag{7}$$

Dividing Equation (6) by 2 and subtracting from Equation (7),

$$(0.141/0.799)^2 - 0.5 \times (0.246/1.022)^2 = (0.046)^2 = (\sigma_f/f)^2 + (\sigma_C/C)^2 + 0.5 \times (\sigma_\gamma/\gamma)^2. \tag{8}$$

Thus we can derive the upper limit of $(\sigma_f/f) \leqslant 4.6\%$ by putting $\sigma_C = \sigma_\gamma = 0$. Taking reasonable values for (σ_C/C) and (σ_γ/γ) of 4% and 1% reduces the estimated uncertainty to $(\sigma_f/f) = 2.3\%$.

From the above, we find that the error in the open solar flux estimates, introduced by using the "*Ulysses* result" of the latitudinal independence of the radial heliospheric field is at most 4.6% and a best estimate is around 2.5% (at the 1σ level). These are both slightly lower than the estimate of 5% for this uncertainty made by Lockwood et al. (2004).

Note that this error is inherent in the use of Equation (1). When computing the open solar flux F_S (usually defined as the flux threading the coronal source surface at $r = r_o = 2.5\ R_\odot = 2.5/215$ AU, where $R_\odot$ is the mean solar radius), one needs to both assume Equation (1) and to make a kinematic correction of $\Delta F_S = 2\pi r^2 \Delta B_r$ to F_{Sr} to allow for the effect of longitudinal structure in the solar wind speed, $F_S = 2\pi r_o^2 |B_r|_{r=ro} = 2\pi r^2(|B_r| - \Delta B_r) = F_{Sr} - \Delta F_S$ (Lockwood et al. 2009a, 2009b, 2009c). The uncertainty in ΔF_S is not included in the uncertainty quoted above which relates only to the assumption of the radial uniformity of the heliospheric field. Because the spread in Figure 12(c) appears to be predominantly due to the variability of the kinematic flux excess effect at $r_1 = 1$ AU, we infer that the spread in 27 day estimates of the open solar flux due to the kinematic effect is $\sigma_1 = (\sigma/2^{0.5}) \approx 0.174$ (the value of $\sigma = 0.246$ for Figure 12(a) contains the effect on both of the two radial field measurements). In annual means this gives an error in the mean of $(\sigma_1/N^{0.5}) = 0.048$, i.e., about 5%.

The analysis of solar cycle effects is difficult because the lifetime of missions and the motion of long-lived missions like *Voyager* mean that the sampling is uneven and the strong dependence on the heliocentric distance r can be aliased with any solar cycle effects. This effect is severe in the available data outside $r > 6$ AU. Even inside $r < 6$ AU care must be taken because the sampling is not uniform, particularly at high latitudes.

Our survey indicates that the flux excess effect is largely restricted to the streamer belt and is greatest during the declining phase of the solar cycle. This is likely to have influenced the large excess fluxes seen in the far heliosphere as they were recorded by *Voyager* and *Pioneer 11* during the declining phase. At sunspot maximum, the high latitude regions become similar to low latitudes and the radial fields are enhanced by the kinematic effect of solar wind stream speed variability at all latitudes. Thus to measure the open solar flux threading the coronal source surface from in situ observations of the radial field, a kinematic correction to the observed radial field must be applied to most observations (including all from near the Earth) before Equation (1) can be applied. Lockwood et al. (2009c) discuss how this is done and how it is also achieved with reasonable accuracy by using the averaging timescale $T = 1$ day. The only measurements for which this correction is not needed are from sunspot minimum and outside the streamer belt at high heliographic latitudes. Reconstructions of centennial variations of open solar flux from geomagnetic activity essentially use the Earth as a spacecraft at $r \approx 1$ AU, $\Delta\Lambda = 0$ and $\Delta\Phi = 0$ (Lockwood et al. 1999a, 1999b; Rouillard et al., 2007). Because Earth is within, or near the edge of the streamer belt at all times, the kinematic correction must be applied in at all times in these reconstructions (Lockwood et al 2009c).

We are grateful to the great many scientists who made possible the recording, storing, and distribution of the heliospheric magnetic field data from many spacecraft that are employed in this paper. The near-Earth interplanetary data were supplied by the OMNI web pages of the Space Physics Data Facility at NASA/Goddard Space Flight Center. We thank several scientists, and in particular Alexis Rouillard, for highly valuable discussions of this research which was supported by the UK Science and Technology Facilities Council.

REFERENCES

Acuña, M. H., Russell, C. T., Zanetti, L. J., & Anderson, B. J. 1997, J. Geophys. Res., 102, 23751
Acuña, M., et al. 2007, Space Sci. Rev., 136, 203
Balogh, A., Smith, E. J., Tsurutani, B. T., Southwood, D. J., Forsyth, F. J., & Horbury, T. S. 1995, Science, 286, 1007
Balogh, A., et al. 1992, A&AS, 92, 221
Behannon, K. W. 1968, J. Geophys. Res., 73, 907
Behannon, K. W., et al. 1977, Space Sci. Rev., 21, 235
Burlaga, L. F., & Barouch, E. 1976, ApJ, 203, 257
Crooker, N. U., Gosling, J. T., & Kahler, S. W. 2002, J. Geophys. Res., 107, SH3-1
Fairfield, D. H. 1969, J. Geophys. Res., 74, 3541
Fairfield, D. H. 1974, J. Geophys. Res., 79, 1368, 1974
Fairfield, D. H., & Ness, N. F. 1972, J. Geophys. Res., 77, 611
Fisk, L. A. 1996, J. Geophys. Res., 101, 15547
Fisk, L. A., & Schwadron, N. A. 2001, ApJ, 560, 425
Fisk, L. A., Zurbuchen, T. H., & Schwadron, N. A. 1999, Space Sci. Rev., 87, 43
Fitzenreiter, R. J., Ogilvie, K. W., Chornay, D. J., & Keller, J. 1998, Geophys. Res. Lett., 25, 249
Frandsen, A. M. A., Connor, B. V., van Amersfoort, J., & Smith, E. J. 1978, IEEE Trans. Geosci. Electron., 16, 195
Hedgecock, P. C. 1975, Space Sci. Instrum., 1, 74
Kokubun, S., Yamamoto, T., Acuña, M., Hayashi, K., Shiokawa, K., & Kawano, H. 1994, J. Geomag. Geoelectr., 46, 7
Larson, D. E., et al. 1997, Adv. Space Res., 20, 655
Lean, J., Wang, Y.-M., & Sheeley, N. R. Jr. 2002, Geophys. Res. Lett, 29, 2224

Lepping, R. P., et al. 1995, Space Sci. Rev., 71, 207
Lockwood, M. 2001, J. Geophys. Res., 106, 16021
Lockwood, M. 2003, J. Geophys. Res., 108, 1128
Lockwood, M. 2004, in The Sun, Solar Analogs and the Climate, ed. I. Redi, M. Güdel, & W. Schmutz (Berlin: Springer), 107
Lockwood, M., & Fröhlich, C. 2007, Proc. R. Soc. A, 463, 2447
Lockwood, M., Forsyth, R. B., Balogh, A., & McComas, D. J. 2004, Ann. Geophys, 22, 1395
Lockwood, M., Owens, M., & Rouillard, A. P. 2009a, J. Geophys. Res, submitted
Lockwood, M., Owens, M., & Rouillard, A. P. 2009b, J. Geophys. Res., submitted
Lockwood, M., Rouillard, A. P., & Finch, I. D. 2009c, ApJ, 700, 937
Lockwood, M., Rouillard, A. P., Finch, I. D., & Stamper, R. 2006, J. Geophys. Res., 111, A09109
Lockwood, M., Stamper, R., & Wild, M. N. 1999a, Nature, 399, 437
Lockwood, M., Stamper, R., Wild, M. N., Balogh, A., & Jones, G. 1999b, Astron. Geophys., 40, 4.10
McComas, D. J., Elliott, H. A., Schwadron, N. A., Gosling, J. T., Skoug, R. M., & Goldstein, B. E. 2003, Geophys. Res. Lett., 30, 1517
McCracken, K. G. 2007, J. Geophys. Res., 112, A09106
Mish, W. H., et al. 1964, J. Geophys. Res., 69, 3531
Mish, W. H., & Lepping, R. P. 1976, Magnetic Field Experiment Data Processing System: Explorers 47 and 50 (Greenbelt, MD: NASA)
Ness, N. F., Behannon, K. W., Scearce, C. S., & Cantarano, S. C. 1967, J. Geophys. Res., 72, 5769
Ness, N. F., Scearce, C. S., & Cantarano, S. C. 1966, J. Geophys. Res., 71, 3305
Ness, N. F., Scearce, C. S., & Seek, J. B. 1964, J. Geophys. Res., 69, 3531
Owens, M. J., Arge, C. N., Crooker, N. U., Schwadron, N. A., & Horbury, T. S. 2008a, J. Geophys. Res., 113, A12103
Owens, M. J., & Crooker, N. U. 2007, J. Geophys. Res., 112, A06, 106
Owens, M. J., Crooker, N. U., & Schwadron, N. A. 2008b, J. Geophys. Res., 113, A11104
Owens, M. J., Schwadron, N. A., Crooker, N. U., Hughes, W. J., & Spence, H. E. 2007, Geophys. Res. Lett., 34, L06104
Petrinic, S. M., & Russell, C. T. 1993, J. Geophys. Res., 98, 18, 963
Rouillard, A. P., Lockwood, M., & Finch, I. D. 2007, J. Geophys. Res., 112, A05103
Russell, C. T., Snare, R. C., Means, J. D., & Elphic, R. C. 1980, IEEE Trans. Geosci. Remote Sens., GE-18, 32
Scearce, C., Cantarano, S., Ness, N., Mariani, F., Terenzi, R., & Burlaga, L. 1975, The Rome-GSFC magnetic field experiment for Helios A and B (E3), Tech. Rep. X -692–75-112 (Greenbelt, MD: NASA)
Schrijver, C. J., DeRosa, M. L., & Title, A. M. 2002, ApJ, 577, 1006
Sheeley, N. R. Jr., & Wang, Y.-M. 2001, ApJ, 562, L107
Smith, C. W., et al. 1998, Space Sci. Rev., 86, 613
Smith, E. J., & Balogh, A. 1995, Geophys. Res. Lett., 22, 3317
Smith, E. J., & Balogh, A. 2003, in Solar *Wind* Ten, ed. M. Velli, R. Bruno, & F. Malara (Washington, USA: American Institute of Physics), 67
Smith, E. J., Balogh, A., Forsyth, R. J., & McComas, D. J. 2001, Geophys. Res. Lett., 28, 4159
Smith, E. J., Connor, B. V., & Foster, G. T. Jr. 1975, IEEE Trans. Magn., 11, 962
Smith, E. J., et al. 2003, Science, 302, 1165
Solanki, S. K., Schüssler, M., & Fligge, M. 2000, Nature, 480, 445
Solanki, S. K., Schüssler, M., & Fligge, M. 2001, A&A, 383, 706
Stayzhkin, V., Yeroshenko, E., & Zakhanov, P. 1985, in Magnetic field experiment in the Intershock project Intershock Project, ed. S. Fischer (Prague: Astron. Inst. Czech. Acad. Sci), 202
Suess, S. T., Phillips, J. L., McComas, D. J., Goldstein, B. E., Neugebauer, M., & Nerney, S. 1998, Space Sci. Rev., 83, 75
Suess, S. T., & Smith, E. J. 1996, Geophys. Res. Lett., 23, 3267
Suess, S. T., Smith, E. J., Phillips, J., Goldstein, B. E., & Nerney, S. 1996, A&A, 316, 304
Svalgaard, L., Cliver, E. W., & Le Sager, P. 2004, Adv. Space Sci., 34, 436
Svalgaard, L., Cliver, E. W., & Le Sager, P. 2003, Geophys. Res. Abstr., 5, 07616 (http://www.cosis.net/abstracts/EAE03/07616/EAE03-J-07616.pdf)
Svalgaard, L., & Cliver, E. W. 2005, J. Geophys. Res., 110, A12103
Svalgaard, L., & Cliver, E. W. 2007, ApJ, 661, L203
Wang, Y.-M., Lean, J., & Sheeley, N. R. Jr. 2000, Geophys. Res. Lett., 27, 505
Wang, Y.-M., Lean, J., & Sheeley, N. R. Jr. 2005, ApJ, 625, 522
Wang, Y.-M., & Sheeley, N. R. Jr. 1995, ApJ, 447, L143
Wang, Y.-M., & Sheeley, N. R. Jr. 2002, J. Geophys. Res., 107, 1302
Wang, Y.-M., & Sheeley, N. R. Jr. 2003, ApJ, 599, 1404
Wang, Y.-M., Sheeley, N. R. Jr., Howard, R. A., Rich, N. B., & Lamy, P. L. 1999, Geophys. Res. Lett., 26, 1349